Urban Fluid Dynamics

Impact of the Numerical Domain on Turbulent Flow Statistics: Scalings and Considerations for Canopy Flows

2023   *A. S. Sathe, M. G. Giometto*

Banner appropriate to article type will appear here in typeset article

Impact of the numerical domain on turbulent flow statistics: scalings and considerations for canopy flows

Atharva S. Sathe[1], Marco G. Giometto[1]†

[1]Department of Civil Engineering and Engineering Mechanics, Columbia University, New York, NY 10027

Large Eddy Simulations (LES) are widely used to study the effects of surface morphology on turbulence statistics, exchange processes, and turbulence topology in urban canopies. However, as LES are only approximations of reality, special attention is needed for the computational model setup to ensure an accurate representation of the physical processes of interest. This paper shows that the choice of the numerical domain can significantly impact the accuracy of turbulent flow statistics, potentially causing a mismatch between numerical studies and experimental data. The study examines the influence of cross-stream aspect ratio (YAR), streamwise aspect ratio (XAR), and scale separation (SS) on first and second-order flow statistics and turbulence topology. It is found that domains with a low YAR underestimate the velocity variance, while those with a low XAR overestimate the variance value. The study proposes a new approach based on the Buckingham Pi theorem to evaluate the effect of SS, as the existing method has major limitations for canopy flows. The results suggest that domains with small SS underpredict the variance value. To minimize the artificial impact of the numerical domain on turbulent flow statistics, the study recommends guidelines for future research, including a YAR of 3 or more, an XAR of 6 or more, and an SS of 12 or more. Error tables are presented to allow researchers to select smaller domains than recommended, depending on their research interests in specific parts of the flow.

Key words: Authors should not enter keywords on the manuscript, as these must be chosen by the author during the online submission process and will then be added during the typesetting process (see Keyword PDF for the full list). Other classifications will be added at the same time.

1. Introduction

The urbanization process profoundly impacts the urban boundary layer (UBL) due to impervious man-made structures that alter the aerodynamic and hydrothermal properties of the land surface. These changes affect mass, energy, and momentum transfer with the

† Email address for correspondence: mg3929@columbia.edu

Abstract must not spill onto p.2

overlying atmosphere, which are the main drivers of urban weather and climate variability. These exchange processes play a crucial role in applications related to urban climate (Oke *et al.* 2017; Oke 1982), urban ecohydrology (Meili *et al.* 2020), air quality (Fernando *et al.* 2001), urban resilience (Gorlé *et al.* 2015), and public health (Lowe & Forsberg 2011), to name a few. The interaction between the urban environment and atmospheric turbulence regulates these exchanges over a broad continuum of scales, ranging from tens of meters over the roof of a building to the kilometer scale over an urban neighborhood (Rotach 1993, 1999). Motivated by the need to address open challenges in these fields and improve our interaction with the environment, the past decades have seen significant efforts to advance our understanding and ability to model turbulent transport in urban settings.

Scientific discovery in the field of microscale meteorology has historically relied on three pillars: field observations (Rotach *et al.* 2005), wind-tunnel experiments (Barlow *et al.* 2004), and numerical simulations (Coceal *et al.* 2006). This paradigm has provided useful insight into how urban morphology affects flow statistics in the UBL, but the alignment between findings from these three fields is not always optimal. An instance of this is where a range of values for the von Kármán constant κ have been proposed by different field measurements and laboratory studies, with values varying from 0.33 to 0.43. This is comprehensively documented by Andreas *et al.* (2006). In addition, Philips *et al.* (2013) have pointed out several challenges in matching parameters of the underlying system, which hinder the accurate alignment of experimental data with numerical simulations. One such obstacle is the use of different methods to compute the repeating parameters, such as friction velocity, which cannot be uniformly applied across different fields. They also demonstrate that the vertical profile of the experimental data can often be accurately matched up to a certain height above the ground, beyond which significant deviations occur. This partial matching approach has also been utilized in other research studies, (see, e.g., Coceal *et al.* 2007; Xie *et al.* 2008), which serves to delimit the region of interest. Another factor contributing to the discrepancy between profiles is the sensitivity of flow statistics to changes in initial and boundary conditions and input parameters. This phenomenon often makes it challenging to establish connections between research findings within the same field (see, e.g., Wang *et al.* 2011).

In the context of numerical simulations, direct numerical simulations (DNS) and large eddy simulations (LES) of open channel flow over surface-mounted cuboids have been the workhorse for studying turbulent transport in the UBL (Coceal *et al.* 2006; Xie & Castro 2006; Leonardi & Castro 2010; Claus *et al.* 2012; Yang & Anderson 2017; Schmid *et al.* 2019; Stroh *et al.* 2020). In these simulations, in addition to the aforementioned sources of discrepancies, one crucial factor affecting the accuracy and reliability of model results is the selection of the numerical domain size (Moin & Kim 1982; Lozano-Durán & Jiménez 2014). Wall-bounded turbulence is characterized by coherent structures with a high correlation in the streamwise direction and a lower but still non-negligible correlation in the spanwise direction. Thus, excessive periodization in the horizontal directions can compromise the accuracy with which these structures are captured (Moin & Kim 1982). Furthermore, in real-world environments, the scale separation between the inversion layer and the height of the canopies is often significant, and the presence of a free-lid top boundary condition too close to the surface may result in spurious effects encompassing the entire UBL. Hence, it is crucial to exercise caution during the simulation design stage to ensure the precise capturing of statistics in the region of interest.

Past DNSs and LESs have been conducted using a range of computational domains, whose size is typically dictated by the available computational resources (Coceal *et al.* 2006; Xie & Castro 2006; Stroh *et al.* 2020). To facilitate the comparison of the various domain sizes used, the concept of aspect ratio and scale separation is employed in this study. The naming

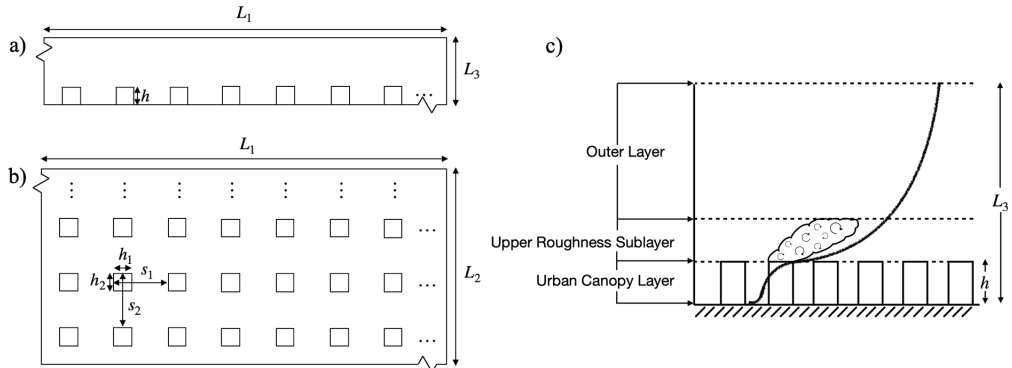Figure 1: (*a*) Side view and (*b*) top view of the computational domain. (*c*) Marks the regions defined as Urban Canopy Layer (UCL), Upper Roughness Sublayer (URSL) and the Outer Layer (OL).

convention used to describe the dimensions of the computational domain is graphically illustrated in figure 1, with the subscripts 1, 2, and 3 referring to the streamwise, cross-stream, and vertical directions, respectively. The aspect ratio of a 3D computational domain is defined as $L_1/L_3:L_2/L_3:1$, where L_1/L_3 defines the streamwise aspect ratio (XAR) and L_2/L_3 defines the cross-stream aspect ratio (YAR). Additionally, the height of the domain is described in terms of the scale separation (SS), defined as L_3/h, where h is the mean height of the underlying surface topography.

One of the early DNS studies of flow over cuboids was performed by Coceal *et al.* (2006) to analyze turbulent flow statistics and unsteady effects in the roughness sublayer (RSL). This study represents a pivotal contribution to the understanding of canopy flow dynamics, achieved through the use of high-resolution DNS. However, as is common in such studies, the need for high resolution necessitated the selection of a smaller domain to ensure computational feasibility. For their open channel flow setup, they used a numerical domain with an aspect ratio of 1:1:1 with an SS of 4. To showcase domain size independence, they compared selected statistics with a domain of aspect ratio 2:2:1 and found the first-order statistics as well as second-order Reynolds stress $\overline{u_1'u_3'}$ to match well. However, it is well known that the profile of $\overline{u_1'u_3'}$ in the bulk of the flow is primarily determined by the imposed pressure gradient and has to vary linearly, as seen from the Navier-Stokes streamwise momentum balance equation; hence the accurate collapse of $\overline{u_1'u_3'}$ for domains with the same boundary layer height does not necessarily indicate the accurate capturing of other second-order moments. Also, as the focus of this study was on the canopy configurations with high packing density, the domain used cannot be deemed as sufficient for the shown statistics to study RSL dynamics in general, as the extent of the RSL, as well as the turbulence characteristics of the RSL depend on the underlying surface configuration (Chung *et al.* 2021). Xie & Castro (2006) performed LES simulations with domain 1:1:1 and SS of 4 and found that their simulations were underpredicting the streamwise RMS velocity (u_{rms}) when compared to corresponding DNS as well as experimental results. Later in this study (§3.1), it will be shown that this underprediction is due to a direct consequence of limiting YAR of the domain and not due to differences between LES and DNS algorithms. Leonardi & Castro (2010) used various domain sizes with SS of 8 and aspect ratios ranging from 1:0.75:1 to 1.25:1.25:1 using DNS. The choice of XARs and YARs was purely driven by the need to accommodate a sufficient number of repeating patterns for different configurations. Schmid *et al.* (2019) used a domain with SS of 4 and aspect ratio 1.5:1.5:1 to study the impact of solid

4

volume fraction on turbulent flow statistics using LES. Yang & Anderson (2017) used LES
to analyze the physics of roughness-induced secondary flows by using domains with SS of 15
and 20 while keeping the aspect ratio of the domain as π:π:1. They showcased that domain
with aspect ratio 2π:2π:1 produces similar results. However, this choice of high SS and high
aspect ratio to reduce the artificial impacts of the numerical domain resulted in fewer nodes
being used to resolve the cubes, which introduces an additional source of error. Stroh *et al.*
(2020) used DNS to study the polarity of secondary flows by using a domain with an SS of
23.25 and an aspect ratio of 8:4:1. These studies demonstrate an apparent disparity in the
employed domain sizes. From these observations, we infer the presence of a general trend
towards maintaining a similar extent of the domain in both the streamwise and cross-stream
directions. However, due to the asymmetrical nature of the turbulent flow structures and their
extended presence in the streamwise direction compared to the cross-stream direction, it
remains uncertain whether these domains will have an artificial impact on the flow statistics.

The presence of roughness-induced secondary flows, a topic which has received increased
attention over the past decade (Willingham *et al.* 2014; Anderson *et al.* 2015; Vanderwel
& Ganapathisubramani 2015; Yang & Anderson 2017; Chung *et al.* 2018; Wangsawijaya
et al. 2020; Stroh *et al.* 2020; Salesky *et al.* 2022), also calls for special attention when
designing the domain size. When the cross-stream spacing between the roughness elements
is sufficiently large, it results in streamwise-aligned time-invariant counter-rotating vortices
predominantly occupying the RSL. The size of these vortices is influenced by both the
spacing of roughness elements in the cross-stream direction and the height of the domain.
As demonstrated (see §3.3), these circulations significantly affect the flow dynamics and
necessitate a specialized approach to evaluate the effect of SS, as the height of the domain
plays a critical role in governing these flows.

In the context of channel flow over aerodynamically smooth surfaces, analysis done by
Comte-Bellot (1963) and Schumann (1973) guided early numerical studies to determine
the optimal domain size to reduce the artificial impact of periodic boundary condition in
the horizontal directions (Moin & Kim 1982). Comte-Bellot (1963) conducted two-point
correlation measurements of velocity fluctuations and found that the correlation became
negligible at a separation of 3.2δ in the streamwise direction and 1.6δ in the cross-stream
direction, where δ is the height of the half channel. Schumann (1973) and Moin & Kim (1982)
later suggested that to reduce the artificial impact of periodic boundary conditions, the size of
the simulation domain should be approximately twice as large as these dimensions. Lozano-
Durán & Jiménez (2014) conducted an extensive domain size analysis for plain channel flow
using DNS at $Re_\tau = 4200$. They showed that the computational box with aspect ratio 2π:π:1
was able to capture the one-point statistics with satisfactory accuracy. This aspect ratio of the
domain aligns with the arguments provided by Schumann (1973) and Moin & Kim (1982).
Zheng *et al.* (2021) conducted a series of LES to examine the impact of domain size on
pollutant dispersion in street canyons with periodic boundary conditions applied only in the
cross-stream direction. The study recommends a SS of 7.5 with a width of at least $0.33L_3$,
an upstream domain length of $0.67L_3$, and a downstream domain length of $1.33L_3$. These
guidelines, however, are based on the 2.5D geometry of cross-stream-aligned bars and cannot
be generalized to LES simulations of open channel flow over cuboids or more general surface
morphologies. As a result, there are currently no comprehensive guidelines for determining
the appropriate size of the numerical domain for studying the UBL using an open channel
flow setup with LES.

The appropriateness of the domain size also depends on the specific region of interest
under investigation. In the existing literature, it is commonly observed that researchers prefer
smaller domain sizes when focusing on regions close to the surface, as capturing accurate
statistics for the entire domain is not always necessary (Anderson 2016; Zhang *et al.* 2022). In

166 this study, we introduce the Urban Canopy Layer (UCL), Upper Roughness Sublayer (URSL),
167 and Outer Layer (OL) as illustrated in Figure 1(c) to facilitate the examination of flow statistics
168 on a per-layer basis. Here, URSL is defined as a distinct component of the RSL, separate from
169 the UCL, to avoid overlap when comparing flow statistics. Notably, we intentionally omit the
170 inertial sublayer in our error analysis, as the study examines diverse packing densities and
171 scale separations, where the presence of an inertial sublayer is not always guaranteed. We
172 discuss this aspect in § 3.4. Hence, we incorporate the inertial sublayer, whenever present,
173 in the OL for the purpose of our investigation.

174 This study investigates the impact of numerical domain size in these three distinct layers
175 and addresses the aforementioned knowledge gap by providing extensive guidelines for
176 researchers based on the packing density of the underlying configuration and the region of
177 interest in a given study. The aim is to equip researchers with the essential data necessary for
178 determining the optimal size of their numerical domain in LES simulations of UBL flows,
179 thereby allowing them to predict any changes to their statistical profiles that may occur due
180 to limitations in domain size.

181 The structure of paper is organized as follows: Section 2 outlines the methodology
182 employed in this study, which includes the details of the simulation algorithm (§2.1) and the
183 dimensional analysis and simulation setup (§2.2). The findings and observations from the
184 simulations are presented in Section 3. Finally, Section 4 provides the conclusions drawn
185 from the study.

186 ## 2. Methodology

187 ### 2.1. *Simulation algorithm*

188 A large suite of LES of flow over cuboid arrays is performed in this study using an in-house
189 code (Albertson & Parlange 1999*a*,*b*; Bou-Zeid *et al.* 2005; Chamecki *et al.* 2009; Anderson
190 *et al.* 2015; Fang & Porté-Agel 2015; Li *et al.* 2016; Giometto *et al.* 2016). The filtered
191 Navier-Stokes equations are solved in their rotational form (Orszag & Pao 1975) to ensure
192 the conservation of mass and kinetic energy in the inviscid limit, i.e.,

$$\frac{\partial \tilde{u}_i}{\partial x_i} = 0 \,, \tag{2.1}$$

194

$$\frac{\partial \tilde{u}_i}{\partial t} + \tilde{u}_j \left(\frac{\partial \tilde{u}_i}{\partial x_j} - \frac{\partial \tilde{u}_j}{\partial x_i} \right) = -\frac{1}{\rho} \frac{\partial \tilde{p}^*}{\partial x_i} - \frac{\partial \tau_{ij}^{SGS}}{\partial x_j} - \frac{1}{\rho} \frac{\partial \tilde{p}_\infty}{\partial x_1} \delta_{i1} + \tilde{F}_i \,, \tag{2.2}$$

196 where $\tilde{u}_1$, $\tilde{u}_2$, and $\tilde{u}_3$ are the filtered velocities along the streamwise x_1, cross-stream x_2,
197 and wall-normal x_3 directions, respectively and ρ is the reference density. The deviatoric
198 component of the subgrid-scale (SGS) stress tensor (τ_{ij}^{SGS}) is evaluated via the Lagrangian
199 scale-dependent dynamic (LASD) Smagorinsky model (Bou-Zeid *et al.* 2005). Extensive
200 validation of the LASD model has been carried out in both wall-modeled simulations of
201 unsteady atmospheric boundary layer flow (Momen & Bou-Zeid 2017; Salesky *et al.* 2017)
202 and in simulations of flow over surface-resolved urban-like canopies (Anderson *et al.* 2015;
203 Li *et al.* 2016; Giometto *et al.* 2016; Yang 2016). Viscous stresses are neglected in the current
204 study, and the skin friction is evaluated via an inviscid equilibrium logarithmic law of the
205 wall for flow over aerodynamically rough surfaces (Giometto *et al.* 2016). Neglecting viscous
206 stresses is valid under the assumption that SGS stress contributions are predominantly from
207 the pressure field. $\tilde{p}^* = \tilde{p} + \frac{1}{3} \rho \tau_{ii}^{SGS} + \frac{1}{2} \rho \tilde{u}_i \tilde{u}_i$ is the modified pressure, which accounts
208 for the trace of SGS stress and resolved turbulent kinetic energy. The flow is driven by
209 a spatially uniform pressure gradient. The wall-parallel directions have periodic boundary

210 conditions, while the upper boundary has free-slip boundary conditions. The lower surface
211 represents an urban landscape with uniformly distributed cuboids. To resolve roughness
212 elements, a discrete forcing immersed boundary method (IBM) is used (Mittal & Iaccarino
213 2005; Chester *et al.* 2007; Giometto *et al.* 2016), where an artificial force F_i is employed
214 to bring the velocity to zero within the cuboids. An algebraic equilibrium wall-layer model,
215 based on the law of the wall, is applied over a narrow band at the fluid-solid interface.

216 The spatial derivatives in the wall-parallel directions are computed by utilizing a pseudo-
217 spectral collocation method that relies on truncated Fourier expansions (Orszag 1970).
218 Conversely, in the wall-normal direction, a second-order staggered finite difference scheme is
219 implemented. The time integration process involves the adoption of a second-order Adams-
220 Bashforth scheme. To deal with non-linear advection terms, the 3/2 rule is utilized for de-
221 aliasing (Canuto *et al.* 2007; Margairaz *et al.* 2018). Additionally, to ensure the enforcement
222 of the incompressibility condition (2.1), a fraction step method (Kim & Moin 1985) is
223 employed.

224 A large number of domain sizes are considered to study the impact of YAR, XAR, and
225 SS. The size of the computational domain is $[0, L_1] \times [0, L_2] \times [0, L_3]$, with L_3/h taking
226 values $\{4, 8, 12, 16\}$. Here h is the height of cuboids, kept constant and equal to 1 across all
227 simulations. L_2/L_3 takes values $\{1.5, 3.0, 4.5\}$ while L_1/L_3 takes values $\{3.0, 6.0, 9.0\}$. An
228 aerodynamic roughness length of $z_0 = 10^{-6}h$ is prescribed at the cube surfaces and the lower
229 surface via the wall-layer model. With the chosen value of z_0, the SGS pressure drag is a
230 negligible contributor to the overall momentum balance (Yang & Meneveau 2016). The flow is
231 in fully rough aerodynamic regime with a roughness Reynolds number $Re_\tau \equiv u_\tau h/\nu = 10^5$.
232 The domain is discretized using a uniform Cartesian grid where each cube is resolved using
233 $n_1 \times n_2 \times n_3 = 4 \times 4 \times 8$ for cases shown in table 2 and $n_1 \times n_2 \times n_3 = 6 \times 6 \times 12$ for
234 cases shown in table 3, where n_i denotes the number of collocation nodes per cube edge.
235 The chosen grid resolution ensures that the study is computationally feasible while providing
236 adequate resolution to capture the flow dynamics with large domains. The analysis presented
237 in A shows that the chosen grid resolution yields flow statistics that are accurate up to
238 second-order moments (based on the scope of this study).

2.2. *Dimensional Analysis and Setup of Simulations*

240 This section discusses the setup of simulations and scaling arguments for flow statistics
241 based on a Buckingham Pi theorem rationale. As mentioned in the Introduction, the study
242 aims to analyze the impact of domain geometry on flow statistics, with a lens on the YAR
243 (L_2/L_3), XAR (L_1/L_3), and SS (L_3/h) parameters. To achieve this objective, a suite of LES
244 of flow over cuboid arrays is conducted, programmatically varying input parameters for the
245 problem. Table 1 shows the quantities governing flow statistics; these quantities encompass
246 two fundamental dimensions, length L and time T, so the considered flow system can be
247 completely characterized by a total of $11 - 2 = 9$ Pi groups (Buckingham 1914).

248 Based on the choice of repeating parameters, two different scaling relations can be obtained
249 for the flow statistics. The merits and limitations of each are discussed in the next sections.

2.2.1. *Canopy length-based scaling*

251 In the canopy length-based scaling, the vertical height of cuboids (h) and friction velocity
252 (u_τ) are chosen as repeating parameters. While all length scales are normalized by h, special
253 considerations are needed for L_1 and L_2 as the flow structures in the OL scale with the
254 boundary layer height. By combining Pi groups, L_1 and L_2 can be scaled appropriately with
255 L_3. Therefore, for example, the normalized mean streamwise velocity can be written in terms

Variable	Name	Variable	Name
U	mean streamwise velocity	h_2	cross-stream width of cuboids
u_τ	friction velocity	h_1	streamwise width of cuboids
L_2	cross-stream extent of the domain	s_2	cross-stream length of repeating unit
L_1	streamwise extent of the domain	s_1	streamwise length of repeating unit
L_3	boundary layer height	x_3	vertical height
h	vertical height of cuboids		

Table 1: Variables determining flow characteristics for open channel flow simulations of flow over cuboids.

	cross-stream aspect ratio cases					streamwise aspect ratio cases				
λ_p	L_3/h	L_2/L_3	L_1/L_3	s_2/h	s_1/h	L_3/h	L_2/L_3	L_1/L_3	s_2/h	s_1/h
0.25	16	1.5	6	2	2	16	3.0	3	2	2
0.25	16	3.0	6	2	2	16	4.5	6	2	2
0.25	16	4.5	6	2	2	16	4.5	9	2	2
0.062	16	1.5	6	4	4	16	3.0	3	4	4
0.062	16	3.0	6	4	4	16	4.5	6	4	4
0.062	16	4.5	6	4	4	16	4.5	9	4	4
0.028	16	1.5	6	6	6	16	3.0	3	6	6
0.028	16	3.0	6	6	6	16	4.5	6	6	6
0.028	16	4.5	6	6	6	16	4.5	9	6	6
0.007	16	1.5	6	12	12					
0.007	16	3.0	6	12	12					
0.007	16	4.5	6	12	12					

Table 2: Set of simulations to study the impact of cross-stream and streamwise aspect ratio of the numerical domain on flow statistics. For all the simulations, $h_2/h = h_1/h = 1$.

of non-dimensional groups as:

$$U/u_\tau = f\left(\frac{L_3}{h}, \frac{L_2}{L_3}, \frac{L_1}{L_3}, \frac{h_2}{h}, \frac{h_1}{h}, \frac{s_2}{h}, \frac{s_1}{h}, \frac{x_3}{h}\right). \tag{2.3}$$

In order to study the impact of YAR (L_2/L_3) on the non-dimensional mean streamwise velocity, the set of simulations in table 2 are chosen where for a particular packing density, only the non-dimensional group L_2/L_3 is varied across cases. This variation is achieved by varying the cross-stream length of the domain L_2 while keeping the boundary layer height L_3 constant. In order to minimize the impact of SS, the largest available value of L_3 is chosen. All the simulations have $h_2/h = h_1/h = 1$.

A similar analysis is carried out to study the impact of XAR using the set of simulations in table 2. The variation in L_1/L_3 is achieved by varying L_1 while keeping L_3 constant. Again, the largest value of SS (L_3/h) is chosen to minimize the impact of the blockage effect. While the largest L_2/L_3 among the available values is chosen for domains with $L_1/L_3 = 6$ and 9,

	common dimensionless groups					h scaling		L_3 scaling	
λ_p	L_3/h	L_2/L_3	L_1/L_3	h_1/h	s_1/h	h_2/h	s_2/h	h_2/L_3	s_2/L_3
0.25	4	3.0	6	1	2	1	2	0.0625	0.125
0.25	8	3.0	6	1	2	1	2	0.0625	0.125
0.25	12	3.0	6	1	2	1	2	0.0625	0.125
0.25	16	3.0	6	1	2	1	2	0.0625	0.125
0.062	4	3.0	6	1	4	1	4	0.0625	0.25
0.062	8	3.0	6	1	4	1	4	0.0625	0.25
0.062	12	3.0	6	1	4	1	4	0.0625	0.25
0.062	16	3.0	6	1	4	1	4	0.0625	0.25
0.028	4	3.0	6	1	6	1	6	0.0625	0.375
0.028	8	3.0	6	1	6	1	6	0.0625	0.375
0.028	12	3.0	6	1	6	1	6	0.0625	0.375
0.028	16	3.0	6	1	6	1	6	0.0625	0.375
0.007	4	3.0	6	1	12	1	12	0.0625	0.75
0.007	8	3.0	6	1	12	1	12	0.0625	0.75
0.007	12	3.0	6	1	12	1	12	0.0625	0.75
0.007	16	3.0	6	1	12	1	12	0.0625	0.75

Table 3: Set of simulations to study the impact of scale separation L_3/h of the numerical domain on flow statistics. Two sets of 7 Pi groups are mentioned in the table based on (2.3) and (2.4). Among these, 5 Pi groups are common between both the sets.

$L_2/L_3 = 3.0$ is chosen for cases with $L_1/L_3 = 3$, since 1:3:3 is a very common aspect ratio of the domain found in canopy flow literature.

To study the impact of SS on flow statistics, set of simulations in table 3 are chosen where for a particular packing density, only L_3/h is varied across cases. This variation in L_3/h was achieved by varying the boundary layer height L_3 while keeping the canopy height h constant. It is later shown that $L_2/L_3 = 3$ and $L_1/L_3 = 6$ are large enough such that they do not artificially alter the flow statistics. Hence, these values are chosen while varying the SS.

2.2.2. *Boundary layer height-based scaling*

In boundary layer height-based scaling, the boundary layer height (L_3) and friction velocity (u_τ) are chosen as repeating parameters. While all length scales are normalized by L_3, special considerations are needed for h_1 and s_1. As the displacement distance is determined by the extent to which flow can penetrate the canopy layer, the parameter is significantly influenced by the height of the roughness element (h), gaps between two elements in the streamwise direction (s_1) and the portion of the gap occupied by the roughness element (h_1). Thus, to preserve the displacement distance, it's more appropriate to scale s_1 and h_1 with canopy height h, which can be achieved from a combination of the new set of Pi groups. Also, the normalized parameter h/L_3 can be inverted to have a consistent SS definition throughout the paper.

Therefore, for example, the normalized streamwise velocity can be written in terms of non-dimensional groups as:

$$U/u_\tau = f\left(\frac{L_3}{h}, \frac{L_2}{L_3}, \frac{L_1}{L_3}, \frac{h_2}{L_3}, \frac{h_1}{h}, \frac{s_2}{L_3}, \frac{s_1}{h}, \frac{x_3}{L_3}\right). \tag{2.4}$$

291   One may also choose to normalize h_1 with s_1 and h_2 with s_2 to preserve the extent of
292 roughness element in the repeating unit. The Pi groups presented in (2.4) ensure that the
293 pairs (h_1, s_1) and (h_2, s_2) are normalized by the same length scale, h and L_3 respectively.
294 This automatically preserves h_1/s_1 and h_2/s_2 across cases, eliminating the need to modify
295 these Pi groups further.

296   To study the impact of SS on flow statistics, a new set of simulations is proposed in table 3
297 based on boundary layer height-based scaling. Variation in L_3/h is achieved similarly by
298 varying the boundary layer height L_3 while keeping the canopy height h constant. For the
299 cases with L_3/h = 16, surface geometry contains regularly arranged cubes. However, in
300 order to preserve h_2/L_3 across different SSs, the cross-stream extent of the cuboids h_2 must
301 be adjusted, which results in distortion of the cube geometry. Therefore, as we decrease
302 the domain height, the cuboids become slender in the cross-stream direction, while the
303 streamwise extent of the cuboid remains the same, as it scales with the canopy height h.
304 The motivation for implementing this scaling technique arises from the inadequacies of
305 traditional canopy length-based scaling for canopy flows, which fails to isolate the effects
306 of SS accurately. This alternative approach provides more precise isolation of SS impacts
307 across all packing densities, as explained in § 3.3 and shown in figure 9.

3. Results and observations

309 This section examines the impact YAR, XAR, and SS on selected turbulent flow statistics.
310 Statistics are discussed on a per-layer basis for the three layers depicted in figure 1(c). To
311 estimate the height of the RSL (x_{3r}), we utilize a formula proposed by Chung *et al.* (2021),
312 i.e.,

$$x_{3r} = \frac{s_2}{2} + d \,, \tag{3.1}$$

314 where d is the aerodynamic displacement height of the given surface. Values for d are
315 chosen from the drag center values reported for square configurations in Kanda *et al.* (2004).
316 This estimate is useful in predicting the extent of the RSL *a priori*; however, it tends to
317 overestimate the height of RSL for densely packed configurations. For the purpose of our
318 study, such shifts in the prediction of the extent of RSL have no significant impact on the
319 error magnitudes, thus justifying the use of (3.1). Additionally, an analysis of the existence of
320 an inertial sublayer is also presented in this section for cases with varying scale separations
321 and packing densities.

322   In this study, the operation of time-averaging is denoted by $\overline{(\cdot)}$, while the process of
323 superficial averaging in the horizontal directions is $\langle \cdot \rangle$. A fluctuation from space and time-
324 averaged quantity is denoted by the symbol $(\cdot)'$.

3.1. *Impact of cross-stream aspect ratio*

326 This section discusses the impact of YAR on first and second-order flow statistics as well as
327 on the structure of turbulence through two-point correlation maps.

328   Figure 2 shows profiles of mean streamwise velocity for different YAR values and packing
329 densities. Differences in the profiles can be solely attributed to the artificial effects of the
330 cross-stream width of the domain. Table 4 shows the error norms in different parts of the
331 boundary layer. The results indicate that the velocity profile of the narrow domain (i.e. YAR
332 1.5) can estimate this quantity within 2% error when compared to the velocity profile of the
333 largest domain across all the layers and all the packing densities. Marginal improvements are
334 seen in the error magnitudes when YAR is increased to 3.0.

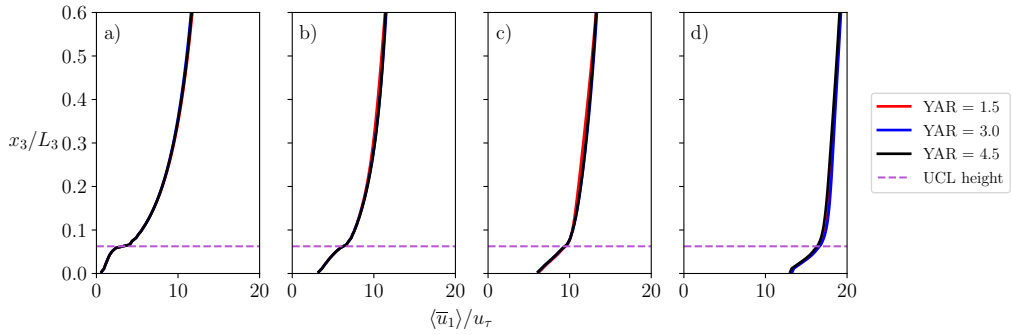335   Figure 3 shows profiles of mean streamwise variance for the same cases considered in

Figure 2: Mean streamwise velocity profiles for different packing densities, (a) 0.25, (b) 0.062, (c) 0.028, (d) 0.007. The vertical profiles for each packing density correspond to different cross-stream aspect ratio cases mentioned in table 2.
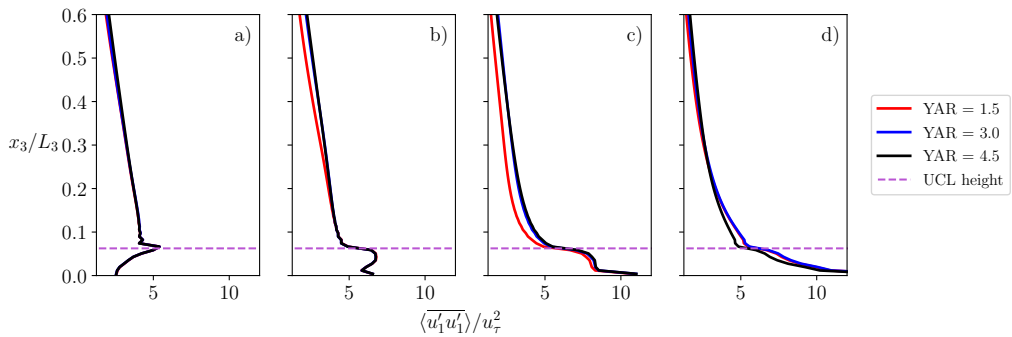

Figure 3: Mean streamwise variance profiles for different packing densities, (a) 0.25, (b) 0.062, (c) 0.028, (d) 0.007. The vertical profiles for each packing density correspond to different cross-stream aspect ratio cases mentioned in table 2.

λ_p	YAR	$\langle \overline{u}_1 \rangle / u_\tau$			$\langle \overline{u_1' u_1'} \rangle / u_\tau^2$			L_{22}		
		UCL	URSL	OL	UCL	URSL	OL	UCL	URSL	OL
0.25	1.5	0.0036	0.0032	0.0116	0.0060	0.0043	0.0543	0.0261	0.0528	0.2048
0.25	3.0	0.0012	0.0004	0.0050	0.0008	0.0031	0.0388	0.0065	0.0163	0.0605
0.062	1.5	0.0014	0.0017	0.0159	0.0036	0.0066	0.1433	0.0414	0.0549	0.3490
0.062	3.0	0.0008	0.0010	0.0094	0.0013	0.0013	0.0203	0.0169	0.0063	0.0787
0.028	1.5	0.0192	0.0165	0.0165	0.0417	0.1722	0.2069	0.0428	0.0325	0.2574
0.028	3.0	0.0020	0.0011	0.0061	0.0088	0.0287	0.0263	0.0067	0.0088	0.0514
0.007	1.5	0.0161	0.0129	0.0090	0.0810	0.0798	0.1477	0.0514	0.0647	0.2187
0.007	3.0	0.0182	0.0195	0.0095	0.0937	0.0874	0.0620	0.0772	0.029	0.0270

Table 4: Relative error (l_2 norm) of mean streamwise velocity, mean streamwise variance and transverse integral length scale in urban canopy layer (UCL), upper roughness sublayer (URSL) and outer layer (OL) for simulations with different cross-stream aspect ratios (YAR). Results from the largest domain (YAR 4.5) are considered as ground truths.

Rapids articles must not exceed this page length

336 figure 2 and errors in the different parts of the boundary layer are shown in table 4. It is
337 observed that in UCL and URSL, the narrow domain is capable of predicting the variance
338 within 10% of the largest domain, except for the case with packing density of 0.028, where
339 the narrow domain results in a noticeable deviation in URSL, leading to an error of 17%.
340 In the OL, the error in this quantity exceeds 14% for all cases except for the densely packed
341 case, for which the error remains within 6%. This observed error can be attributed to the
342 tendency of the narrow domain to underestimate the value of variance. In contrast, the
343 domain with YAR 3.0 can predict this quantity with an error magnitude that is approximately
344 6% or lower when compared to the profiles of the largest domain across all the layers and
345 all the packing densities, indicating a reduced influence of artificial periodization in the
346 cross-stream direction. This also indicates that the periodic boundary condition in the cross-
347 stream direction has a lesser impact on the first-order statistics compared to the second-order
348 statistics. In order to investigate the underlying cause of the observed statistical shifts in
349 the narrow domain, we now use two-point correlation to assess the impact of restricting
350 cross-stream width of the domain on the topology of turbulence.

351   Figure 4 shows two-point correlation (R_{11}) contours and instantaneous flow field fluctu-
352 ations for different YAR at $x_3/L_3 = 0.6$. For brevity, only the cases with packing density
353 of 0.028 are shown here. This packing density is chosen to qualitatively assess the reason
354 behind the narrow domain noticeably underpredicting the mean streamwise variance, as seen
355 in figure 3(c). The color bar is not shown here as the values are not used for inference;
356 however, it is kept constant for all the flow field visualizations to get an appropriate sense
357 of fast (red) and slow (blue) turbulent streaks. The two-point correlation between any two
358 quantities is defined as

$$359 \qquad R_{ij}(\Delta x_1, \Delta x_2, x_3) = \frac{\overline{u_i'(x_1, x_2, x_3)u_j'(x_1 + \Delta x_1, x_2 + \Delta x_2, x_3)}}{\sigma_{u_i}\sigma_{u_j}} \qquad (3.2)$$

360 where σ_{u_i} is the standard deviation of the fluctuating field u_i'. It is important to note that the
361 presence of repeated indices in this context does not denote summation. From figure 4(a, c,
362 e), we see that the streamwise extent of correlation for the narrow domain is much smaller
363 compared to cases with YAR 3.0 and 4.5. This observation is strongly supported by the
364 streamwise instantaneous flow field fluctuations shown in figure 4(b, d, f). For the cases
365 with YAR 3.0 and 4.5, we observe long streamwise turbulent structures of the order of the
366 corresponding domain extent, justifying a more significant streamwise correlation. However,
367 as shown in figure 4(b), no such structures are observed for the case with YAR 1.5. This
368 shows that the narrow cross-stream width of the domain can significantly alter the growth of
369 turbulent flow structures in the streamwise direction.

370   As these coherent structures scale with the separation distance from the wall and as figure 4
371 only illustrates the case where $x_3/L_3 = 0.6$, a more detailed analysis is needed to comment
372 on the suitability of the domain with YAR 1.5 to accommodate a pair of these structures
373 at different vertical positions and across all packing densities (Tomkins & Adrian 2003;
374 Ganapathisubramani *et al.* 2005; Coceal *et al.* 2007). To address this matter, we analyze the
375 typical width of such structures and investigate the ability of the domain with YAR 1.5 to
376 accommodate fast and slow turbulent streaks at different vertical locations.

377   Figure 5 shows the total width of a fast and slow streak pair, which were observed in
378 figure 4(d, f), as a function of height for cases with YAR 3.0 and 4.5. The width of a structure
379 is computed as twice the cross-stream width over which R_{11} drops from 1 to 0. This width is
380 then doubled to get the total width of the fast and slow streak pair. Figure 5 shows that as the
381 size of streamwise coherent structure increases with height, the domain with YAR 1.5 is not
382 sufficient to accommodate a pair of fast and slow streaks at $x_3/L_3 = 0.6$. This explains why
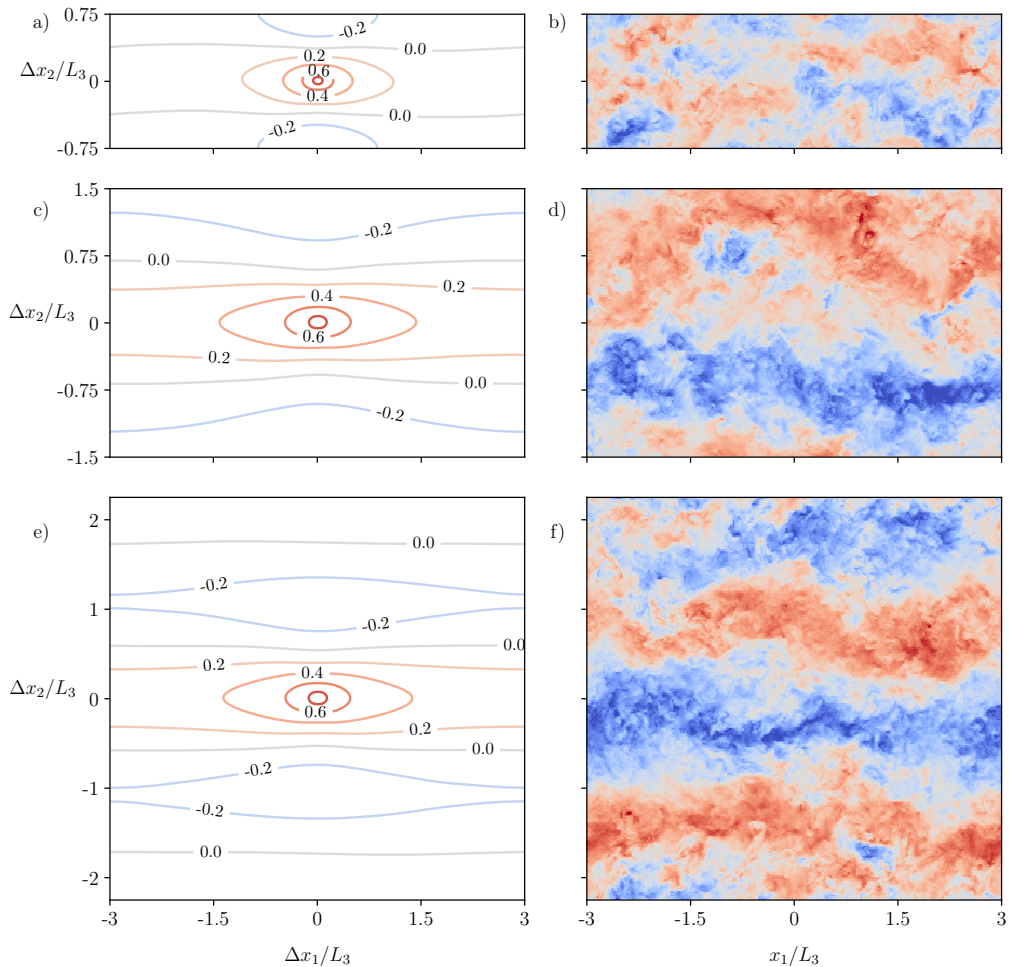
Figure 4: Two point correlation R_{11} contours (a, c, e) and streamwise instantaneous flow field fluctuations (b, d, f) for cases with packing density 0.028. The cross-stream aspect ratio is varied as: (a, b) 1.5, (c, d) 3.0, (e, f) 4.5. The wall-parallel slice shown in all the figures is taken at $x_3/L_3 = 0.6$.

no streamwise coherence was observed in figure 4(b). We also see that till $x_3/L_3 \approx 0.8$, the domain with YAR 3.0 is sufficient to accommodate a fast and slow streak pair even as the cross-stream extent of the domain is increased to YAR 4.5. A rapid increase in the structure size is observed beyond $x_3/L_3 \approx 0.8$ due to the free-lid boundary condition applied at the top of the computational domain, as it inhibits the inclined growth of the structures, conforming them to a planar configuration (Ganapathisubramani *et al.* 2005). Since canopy flow studies in the open-channel flow setup do not typically focus on this region of the boundary layer, YAR 3.0 can be considered good enough to capture these coherent structures in the region below $x_3/L_3 \approx 0.8$. A noticeable deviation can be seen in the width of streamwise coherent structures between cases with YAR 3.0 and 4.5. However, as seen from figure 2, figure 3 and table 4, the impact of this deviation does not significantly alter the first and second order statistics. From figure 5 we also see that the vertical locations at which the width of the fast and slow streak pair exceeds the width of the domain with YAR 1.5 is different for different packing densities. For the case with highest packing density (i.e. 0.25), the crossing
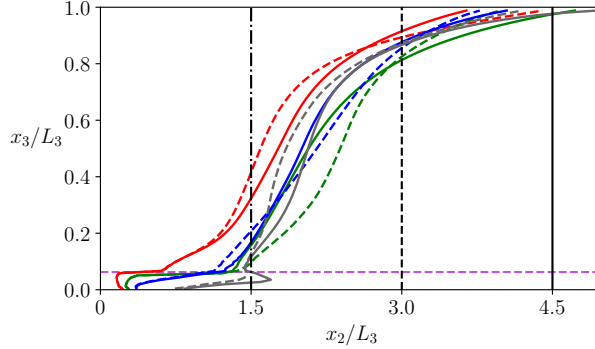
Figure 5: Width of turbulent streamwise coherent structures consisting of fast and slow streak pair. Cases with cross-stream aspect ratio (YAR) of 4.5 are shown in solid lines and YAR of 3.0 in dashed lines. Colors correspond to different packing densities: 0.25 - red, 0.062 - green, 0.028 - blue, 0.007 - grey. Black vertical lines indicate the width of the domain: dash-dot - YAR 1.5, dashed - YAR 3.0, solid - YAR 4.5. Purple horizontal line (dashed) indicates height of the urban canopy layer.
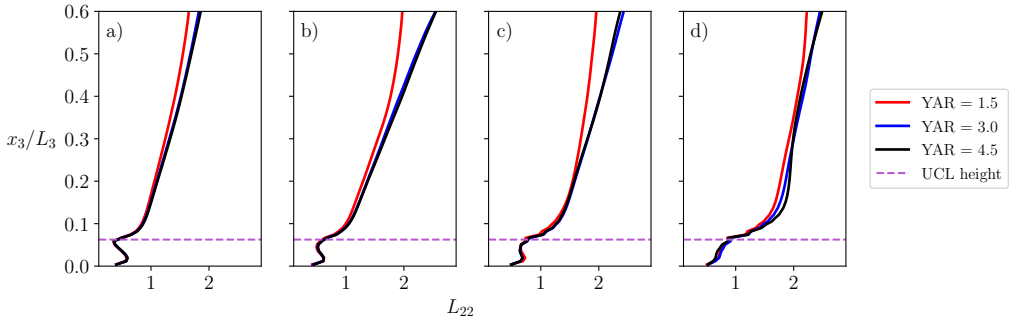

Figure 6: Transverse integral length scale for different packing densities, (a) 0.25, (b) 0.062, (c) 0.028, (d) 0.007. The vertical profiles for each packing density correspond to different cross-stream aspect ratio cases mentioned in table 2.

point lies at $x_3/L_3 \approx 0.37$. For packing densities 0.062 and 0.028, the crossing point lies at $x_3/L_3 \approx 0.15$, whereas this value is $x_3/L_3 \approx 0.07$ for packing density 0.007. Although these structures are seen to be increasing at a similar rate across all packing densities, the different vertical locations of these crossing points are a result of differences in the width of these structures near the top of the canopy layer. As observed by Coceal *et al.* (2007), the size of these structures near the canopy top is influenced by the geometry of obstacles, and their potential for growth depends on the configuration of said obstacles. This explains why different error magnitudes were observed in figure 3 across different packing densities for YAR 1.5, as the same domain width may or may not be able to accommodate these structures at a particular height based on the underlying surface configuration.

So far, the analysis has shown that insufficient cross-stream width of a numerical domain can inhibit the growth of streamwise coherent structures. To analyze the impact of YAR on the cross-stream coherent structures, transverse integral length scale L_{22} is shown in figure 6 as a function of height. Errors in the profiles in different parts of the boundary layer are

14

411 shown in table 4. The integral length scale in this study is defined as

$$L_{ii}(x_3) = \int_0^\infty R_{ii}(\Delta x_1 \delta_{i1}, \Delta x_2 \delta_{i2}, x_3) d\Delta x_i \qquad (3.3)$$

413 Thus, L_{22} characterizes the length of instantaneous flow structures in the cross-stream
414 direction. Note that the presence of repeated indices in this context does not imply summation.
415 To discard the noise present around the correlation value 0, a cutoff value of 0.2 is used to
416 compute the transverse integral length scale (Ganapathisubramani *et al.* 2005). The profile
417 of the narrow domain in the OL exhibits significant deviation across all packing densities,
418 as shown in figure 6, with errors exceeding 20% in all cases. Whereas in UCL and URSL,
419 a maximum of 7% error is observed for the narrow domain. In contrast, the domain with
420 YAR 3.0 is able to predict the length scale within 8% of the values of the profiles with the
421 largest domain across all the layers and packing densities, indicating a reduced influence
422 of cross-stream periodization on the spanwise growth of coherent structures. It is crucial
423 to acknowledge that the two-point correlation function in the RSL cannot be considered
424 independent of the position vector due to the heterogeneity of the flow field. In the RSL,
425 strong signatures from the mean flow patterns affect the values of the integral length scale.
426 Nevertheless, accepting this limitation permits the assessment of domain size impact in these
427 layers based on the observed deviations since the mean flow patterns should have the same
428 effect under identical surface configurations and flow conditions.

429 The extent of R_{22} is often used to see how far the flow field is correlated in the cross-stream
430 direction. For the turbulent channel flow simulation, Moin & Kim (1982) showed that the
431 transverse correlation becomes zero around $1.6L_3$ for a large domain. Based on this, they
432 estimated that a cross-stream domain length of $3.2L_3$ is sufficient to accommodate coherent
433 structures, which is in agreement with the presented results. However, the extent of transverse
434 correlation doesn't always provide a complete picture. As shown in figure 4, the destruction
435 of coherent structures for the narrow domain will also result in a de-correlated flow field,
436 wrongly indicating the domain to be sufficient for de-correlation to occur.

3.2. *Impact of streamwise aspect ratio*

438 This section discusses the impact of XAR of the numerical domain on first and second-order
439 flow statistics as well as on the structure of turbulence through two-point correlation maps.
440 Long structures seen in figure 4 are also a consequence of periodic boundary condition
441 in the streamwise direction. In order to assess the impact of the interactions of these infinite
442 structures, configurations mentioned in table 2 are simulated where the streamwise extent of
443 the domain is varied systematically.
444 Figure 7 shows the R_{11} correlation contours, mean streamwise velocity, mean streamwise
445 variance and longitudinal integral length scale for cases with different XARs. For brevity,
446 only the cases with packing density of 0.028 are shown here. From the figure, we see that
447 as the domain is restricted in the streamwise direction, the correlation that infinite structures
448 can sustain increases due to periodic boundary condition. Figure 7(a) shows that the infinite
449 structure can sustain a positive correlation of 0.4 throughout the domain for the case with
450 XAR 3.0. This value drops to 0.2 as the streamwise extent of the domain is increased, as
451 shown in figure 7(c, e). The same is observed with negative correlation contours where the
452 infinite structures can sustain a -0.2 correlation throughout the domain for cases with XAR
453 3.0 and 6.0, which is not observed for the case with XAR 9.0. Figure 7(b, d, f) shows mean
454 streamwise velocity and variance, as well as the integral length scale L_{11}, which characterizes
455 the length of instantaneous flow structures in the streamwise direction and is computed in
456 accordance with equation 3.3, using a cutoff value of 0.5 (Ganapathisubramani *et al.* 2005).
457 The increased cutoff value, compared to the 0.2 used for L_{22}, ensures that all analyzed cases,
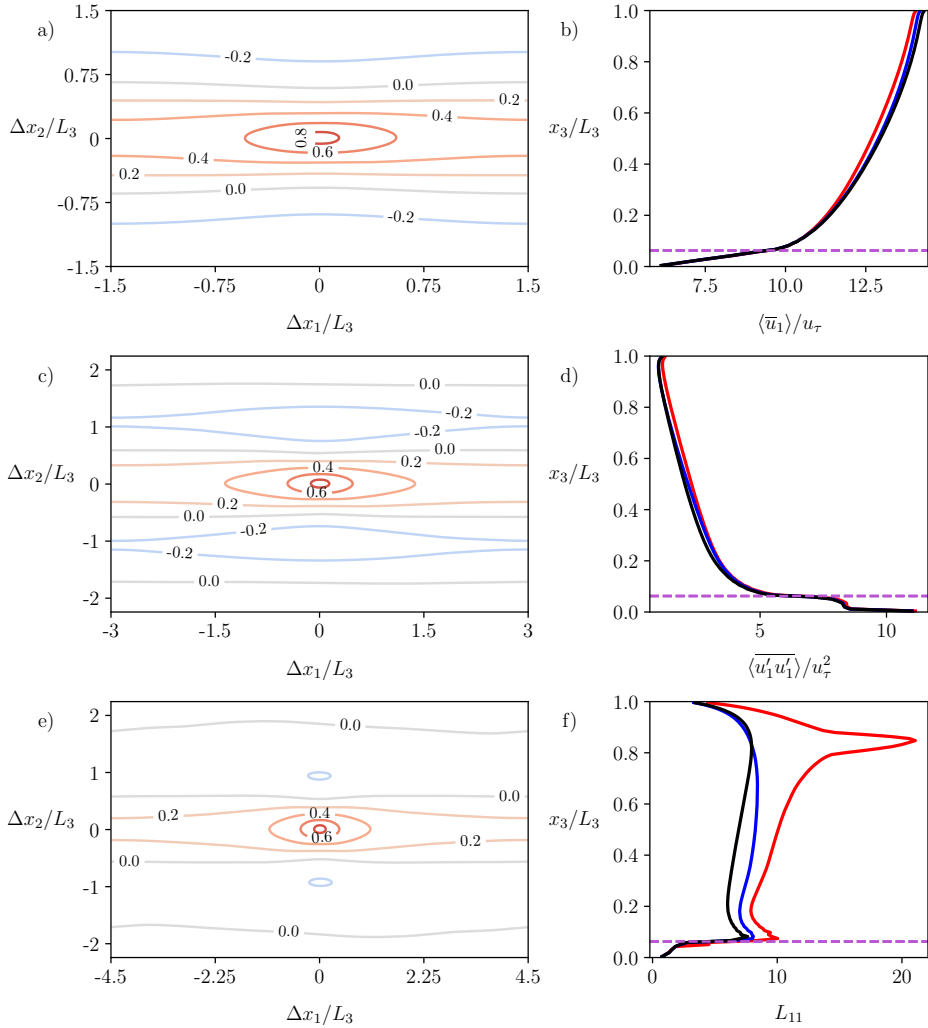
Figure 7: Two point correlation R_{11} contours (a, c, e), mean streamwise velocity (b), mean streamwise variance (d), longitudinal integral length scale (f) for cases with packing density 0.028. The streamwise aspect ratio (XAR) is varied as: (a, b) 3.0, (c, d) 6.0, (e, f) 9.0. For plots (b, d, f), XAR 3.0 is shown in red, 6.0 in blue, and 9.0 in black. The wall-parallel slice shown in (a, c, e) is taken at $x_3/L_3 = 0.6$. Domain configurations for cases with different XAR are shown in table 2. Purple horizontal line (dashed) indicates height of the urban canopy layer.

spanning various domains and packing densities, demonstrate a correlation value below the chosen contour threshold. From these statistics, we see that the strength of correlation resulting from periodization influences the first and second-order statistics. The cases with smaller streamwise extent tend to increase the correlation of the infinite structures throughout the domain, which coincides with increased variance and slower mean streamwise velocity. The decrease in mean streamwise velocity is likely the result of increased turbulent mixing. The case with a shorter domain (i.e. XAR 3.0) was found to produce a mean streamwise velocity prediction that is within 3.5% of the values obtained from the largest domain (i.e. XAR 9.0) across all layers and packing densities, as shown in table 5. The maximum error

λ_P	XAR	$\langle \overline{u}_1 \rangle / u_\tau$			$\langle \overline{u_1' u_1'} \rangle / u_\tau^2$		
		UCL	URSL	OL	UCL	URSL	OL
0.25	3.0	0.0051	0.0082	0.0349	0.011	0.0317	0.1558
0.25	6.0	0.0019	0.0032	0.0074	0.0047	0.007	0.052
0.062	3.0	0.0015	0.0013	0.0258	0.0189	0.0514	0.2015
0.062	6.0	0.0044	0.0040	0.0051	0.0095	0.0104	0.0169
0.028	3.0	0.0054	0.0051	0.0192	0.0194	0.0457	0.1208
0.028	6.0	0.0007	0.00013	0.0062	0.0044	0.0316	0.0584

Table 5: Relative error (l_2 norm) of mean streamwise velocity and mean streamwise variance in urban canopy layer (UCL), upper roughness sublayer (URSL), and outer layer (OL) for simulations with different streamwise aspect ratios (XAR). Results from the largest domain (XAR 9.0) are considered as ground truths.

observed in the mean streamwise variance for the UCL and URSL remains limited to 5% for all cases with the same domain. In contrast, the mean streamwise variance error in the OL can increase up to 20% for the shorter domain. On the other hand, the case with XAR 6.0 is able to predict both the statistics within 6% of the values obtained from the largest domain across all the layers and packing densities, indicating a reduced influence of artificial periodization on first and second-order statistics. This also indicates that the periodic boundary condition in the streamwise direction has a lesser impact on the first-order statistics compared to the second-order statistics.

It is interesting to note that the impact of a restricted streamwise and cross-stream domain extent on flow statistics is entirely the opposite. When the cross-stream width of the domain is restricted, it inhibits the growth of coherent structures, which can lead to lower variance and higher mean streamwise velocity. Conversely, when the streamwise length of the domain is restricted, it enhances the strength of coherent structures due to artificial periodization, resulting in higher variance and lower mean streamwise velocity.

3.3. *Impact of scale separation*

This section discusses the impact of SS (L_3/h) of the numerical domain on first and second-order flow statistics. Here, two different scalings mentioned in §2.2.1 and §2.2.2 are discussed in order to isolate the impact of SS appropriately.

Initially, simulation configurations are selected based on canopy length-based scaling discussed in §2.2.1 to achieve different SSs. The configurations are mentioned in table 3, where non-dimensional groups under the "*h* scaling" column are used together with the common dimensionless groups. This is the conventional way to test the impact of SS, where the domain height is varied systematically without changing the surface.

Figure 8 shows profiles of mean streamwise velocity for different SSs and packing densities. For the case with the highest packing density shown in figure 8(a), all the velocity profiles from SS 8 to 16 collapse quite well. However, this trend is not observed when the packing density of the canopy surface is systematically decreased. Figure 8(b, c, d) show significant deviation in the mean velocity profile when the SS varies from 8 to 16. This significant difference in the velocity profiles is observed for the sparsely packed cases because varying L_3/h while keeping s_2/h constant changes a key parameter s_2/L_3, which controls the size and strength of secondary flows in sparse, regularly aligned canopies (Willingham *et al.* 2014; Yang & Anderson 2017; Vanderwel & Ganapathisubramani 2015). For example, when the
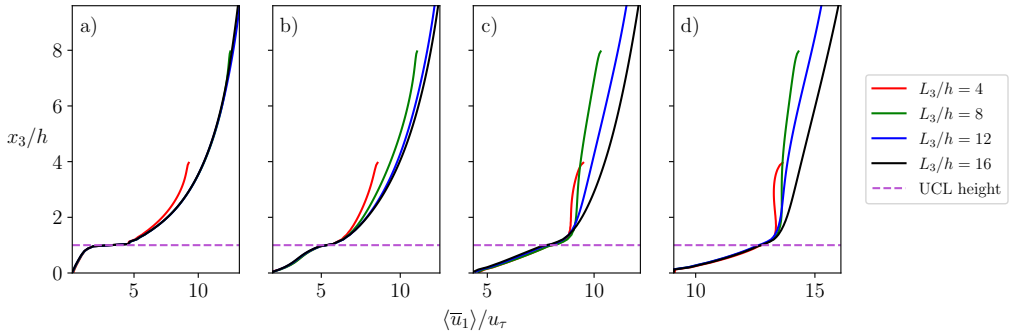
Figure 8: Mean streamwise velocity profiles for different packing densities, (a) 0.25, (b) 0.062, (c) 0.028, (d) 0.007. The vertical profiles for each packing density correspond to different scale separation cases mentioned in table 3, under the h scaling column.
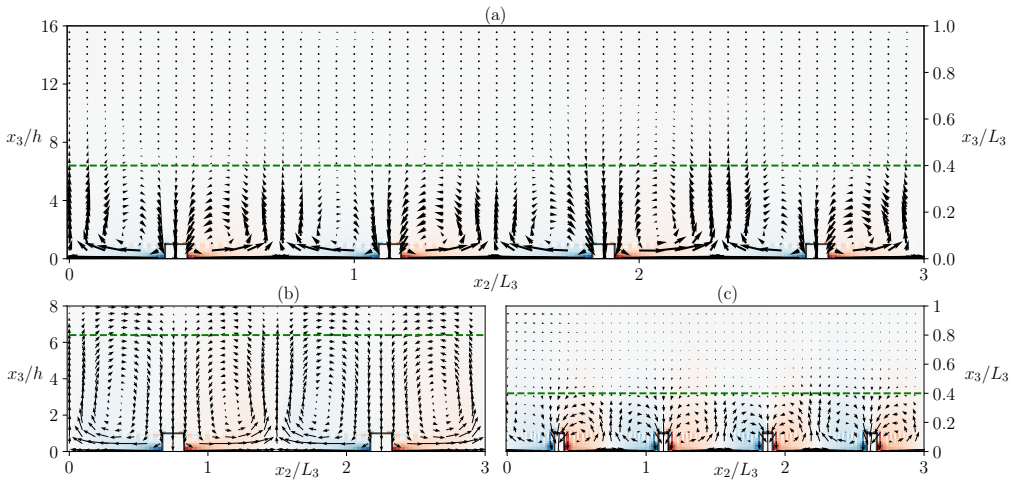

Figure 9: Flow configuration for sparsely arranged canopies based on two different sets of Pi groups. The packing density of the surface is 0.007 in all cases. The scale separation is varied as (a) 16, (b, c) 8. Configuration in (b) is scaled down from (a) based on canopy length-based scaling, whereas configuration in (c) is scaled down from (a) based on boundary layer height-based scaling. The green reference line matches x_3/h for (a) and (b) and x_3/L_3 for (a) and (c).

domain height is decreased from $16h$ to $8h$ for the sparse configuration with packing density 0.007, for which s_2/h is equal to 12, s_2/L_3 changes from 0.75 to 1.5. When s_2/L_3 is 0.75, it results in the generation of moderately strong secondary flows, whereas when the parameter is increased to 1.5, it results in strong secondary flows, which occupy the entire half-channel height. Figure 9 displays this effect. When the base configuration shown in figure 9(a) is scaled down using canopy length-based scaling, the resulting flow configuration shown in figure 9(b) is quite different. A dashed green line is drawn for reference at $x_3/h = 6.4$. We can clearly see that at this height, the flow configuration is entirely different, and the magnitude of this difference is directly related to the size and strength of secondary flows in the base configuration. Hence, the deviation observed in figure 8(b, c, d) cannot be solely attributed to the effect of SS. These results highlight that, for sparse configurations which induce secondary flows, the set of Pi groups stated in (2.3) cannot be used to isolate the
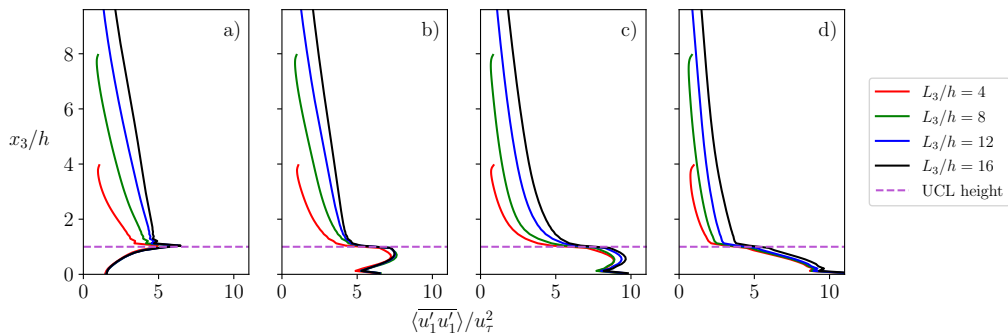
Figure 10: Mean streamwise variance profiles for different packing densities, (a) 0.25, (b) 0.062, (c) 0.028, (d) 0.007. The vertical profiles for each packing density correspond to different scale separation cases mentioned in table 3, under the "h scaling" column.

λ_p	SS	$\langle \overline{u}_1 \rangle / u_\tau$		$\langle \overline{u'_1 u'_1} \rangle / u_\tau^2$	
		UCL	URSL	UCL	URSL
0.25	4	0.0684	0.0280	0.0663	0.3004
0.25	8	0.0431	0.0066	0.0184	0.1273
0.25	12	0.0149	0.0026	0.0073	0.0395
0.062	8	0.0303	0.0272	0.0208	0.1584
0.062	12	0.0080	0.0040	0.0051	0.0528

Table 6: Relative error (l_2 norm) of mean streamwise velocity and mean streamwise variance in urban canopy layer (UCL) and upper roughness sublayer (URSL) for simulations with different scale separations (SS) mentioned under h scaling column in table 3. Results from the tallest domain (SS 16) are considered as ground truths.

511 impact of SS. For the densely packed case, the strength of the secondary flows is very weak
512 due to the limiting cross-stream gap, and the surface essentially behaves as a conventional
513 rough surface (Yang & Anderson 2017). This is why decreasing the parameter s_2/L_3 with
514 increasing domain height doesn't have any impact on already weak secondary flows, which
515 justifies the good collapse of streamwise velocity profiles observed in figure 8(a) across a
516 large range of SS values.
517   Figure 10 depicts profiles of mean streamwise variance for various SSs and packing
518 densities. The figure demonstrates that the rate of variance decay is significantly affected
519 by the top boundary condition. Furthermore, the change in the parameter s_2/L_3 also affects
520 the variance values in the RSL. Yang & Anderson (2017) showed that surfaces with s_2/L_3
521 considerably below 1 behave as conventional rough surfaces and exhibit weaker secondary
522 circulations. Since the secondary flows are weak in such cases, the RSL statistics are
523 predominantly affected by the wake flow from the canopies. Turbulence scales in the wake
524 flow are primarily influenced by the dimensions of the canopy, which are preserved in canopy
525 length-based scaling (Raupach *et al.* 1991). As a result, the turbulence features of the RSL
526 remain similar for these cases, enabling comparisons across different SSs. Hence, this scaling
527 can still be used to evaluate the impact of SS on RSL statistics for cases with packing densities
528 of 0.25 and 0.062 and for scale separations where s_2/L_3 is less than or equal to 0.5. It is
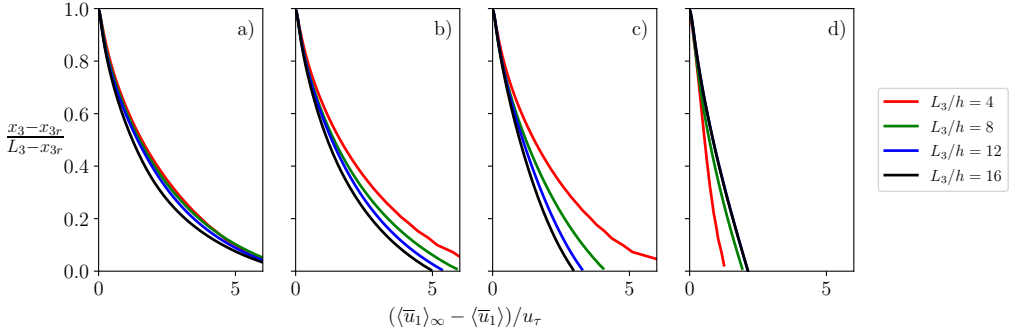529 worth noting, however, that instances with $s_2/L_3 \approx 0.5$ also display minor secondary scale

Figure 11: Mean streamwise velocity defect profiles for different packing densities, (a) 0.25, (b) 0.062, (c) 0.028, (d) 0.007. The vertical profiles for each packing density correspond to different scale separation cases mentioned in table 3, under the L_3 scaling column.

circulations, indicating that the RSL traits may not be identical, but these will not contribute significantly to the flow statistics. The error values of these cases in the UCL and URSL are presented in table 6. The maximum error observed for the mean streamwise velocity is less than 7% across all scale separations. As for the variance, the maximum error observed in the UCL is also less than 7% across all scale separations. In the URSL, the cases with a scale separation of 12 capture this statistic with a maximum error of approximately 5%, while the error can reach up to 15% for the cases with a scale separation of 8 and 30% for the case with a scale separation of 4. The discussion in the last two paragraphs demonstrates that the canopy length-based scaling is unable to accurately isolate the impact of SS on turbulent flow statistics in the sparse cases which generate secondary flows as well as in the outer layer. Although scaling x_3 with L_3 instead of h enables comparison of statistics in the outer layer for selected cases, it still does not facilitate comparison of the statistics for sparse cases or packing density 0.062 with scale separation 4. Thus, to overcome the limitations of canopy length-based scaling and to study the impact of SS across all the packing densities and the outer layer, a change in the repeating parameter determining the length scale is required.

A different scaling was proposed in §2.2.2, where the domain height was chosen as a repeating parameter. This results in a different set of Pi groups presented in (2.4). The effect of this change in the repeating parameter can be appreciated in figure 9. When the base configuration shown in figure 9(a) is scaled down using boundary layer height-based scaling shown in figure 9(c), a similar flow configuration is achieved. A green dashed line is drawn for reference at $x_3/L_3 = 0.4$, which accurately compares the extent of secondary circulation despite having different SS. Figure 9(c) also demonstrates that the underlying surface configuration changes and the cuboids become slender when the SS is decreased as per boundary layer height-based scaling. However, it should be noted that this change in configuration preserves the frontal area fraction of the surface, which results in a similar z_0 value throughout the cases for a fair comparison.

As the length scales of eddies in the RSL are predominantly associated with the canopy lengths, a direct comparison of statistics is not possible in this region, as the boundary layer height-based scaling distorts the surface. However, we can still compare statistics in the OL as it has turbulent eddies independent of canopy scales. Also, the OL turbulence is most affected by the SS due to its close proximity to the no-stress boundary condition. Thus, minimizing the impact of SS in the OL ensures that the impact of SS is minimal in UCL and URSL.

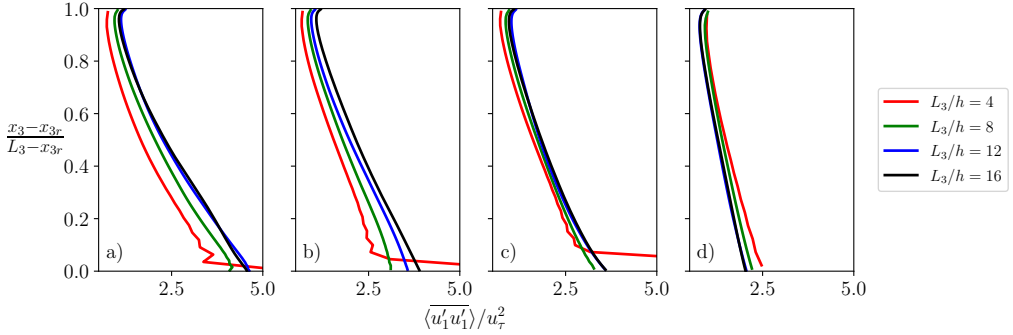In order to accurately match equivalent points in the outer layer across cases, a new scaling

Figure 12: Mean streamwise variance profiles for different packing densities, (a) 0.25, (b) 0.062, (c) 0.028, (d) 0.007. The vertical profiles for each packing density correspond to different scale separation cases mentioned in table 3, under the L_3 scaling column.

	SS - $\langle \overline{u}_1 \rangle / u_\tau$			SS - $\langle \overline{u_1' u_1'} \rangle / u_\tau^2$		
λ_p	4	8	12	4	8	12
0.250	0.1413	0.1269	0.0793	0.2366	0.1047	0.0223
0.062	0.3939	0.2026	0.1004	0.2865	0.1751	0.0775
0.028	0.8532	0.3279	0.1192	0.2773	0.0720	0.0219
0.007	0.4091	0.1268	0.0029	0.1836	0.0950	0.0143

Table 7: Relative error (l_2 norm) of mean streamwise velocity and mean streamwise variance for simulations with different scale separation and packing densities mentioned under L_3 scaling column in table 3. Results from the case with the largest scale separation ($L_3/h = 16$) are considered as ground truths. The statistics are compared in the outer layer (OL).

is introduced, which maps the extent of the outer layer from 0 to 1. A non-dimensional function $f(x_3, x_{3r}, L_3)$ is defined as:

$$f(x_3, x_{3r}, L_3) = \frac{x_3 - x_{3r}}{L_3 - x_{3r}} , \qquad (3.4)$$

where x_{3r} is the height of the RSL, which is calculated from equation 3.1.

Figure 11 shows the mean streamwise velocity defect for different SSs and packing densities. Simulation setups for the shown cases can be found in table 3, where the non-dimensional groups under "L_3 scaling" are considered along with the common dimensionless groups. A converging trend is observed across different packing densities, which was absent in figure 8. Figure 12 shows the mean streamwise variance for the same cases. We observe that the errors between the streamwise velocity and streamwise variance profiles shown in table 7 are relatively smaller for the densely packed case as well as the sparsest configuration considered in this study. A physical explanation for this behavior can be provided by examining the characteristics of the RSL in the distorted surfaces. In canopy flows that do not generate secondary flows, the RSL is dynamically influenced by length scales associated with roughness elements (Raupach *et al.* 1991). Therefore, the change in the dimensions of cuboids required to preserve the s_2/L_3 Pi group changes the RSL characteristics of the surface. When the SS is low, the OL is not truly independent of influence from the roughness elements, and this change in the RSL turbulence also affects statistics in the OL. For the case

with high packing density, the RSL does not extend significantly beyond the UCL, as can be inferred from the magnitude of dispersive fluxes (not shown), and OL independence is quickly achieved. In sparse canopies that generate secondary flows, the RSL is predominantly occupied by the counter-rotating vortices, which are preserved when the surface is scaled as per the boundary layer height-based scaling. Hence, the boundary layer height-based scaling tends to preserve the RSL characteristics for the sparse cases generating secondary flows. This explains the observed lower shift in streamwise velocity and streamwise variance profiles for highly dense and highly sparse cases. From the table, we see that the domains with SS 12 predict both the quantities with less than 12% error in the OL, and this error magnitude is likely to be lesser in UCL and URSL given their relatively more significant separation from the top boundary. In contrast the error for cases with SS 4 and 8 can be substantial and we refer the reader to table 7 for specific values. Also, a monotonic increase is observed in the value of variance as the SS is increased, except for the case with strong secondary flows. This shows that domains with smaller SSs tend to inhibit the growth of turbulent structures, which contribute to the variance magnitude. This behavior is clearly linked to the free-lid upper boundary condition, which is known to dampen velocity fluctuations, especially those in the vertical direction. In cases where strong secondary flows are present, the reversal in the trend indicates that the patterns of strong mean flow in the RSL affect the turbulence in the OL, leading to a higher variance value. However, when the SS is increased beyond 12, the statistics show excellent collapse, suggesting the recovery of OL independence.

3.4. *Existence of inertial sublayer in canopy flows*

In this section, the existence of an inertial sublayer is examined for cases with different SS available from the suite of simulations presented in table 3. In urban boundary layer flow, the inertial sublayer exists between the RSL and OL and is the region where most of the turbulent kinetic energy is generated (Jiménez 2004). A logarithmic rise in the velocity within the region characterizes this layer. In the flow over roughness elements, the logarithmic profile can be described in terms of a roughness function $\Delta u_1/u_\tau$, which quantifies the deviation of the mean streamwise velocity from the logarithmic profile observed in smooth wall flow (Raupach *et al.* 1991), as

$$\frac{\langle \overline{u}_1 \rangle}{u_\tau} = \frac{1}{\kappa}\ln\left(\frac{x_3 - d}{h}\right) + \mathrm{B} - \frac{\Delta u_1}{u_\tau} \,. \tag{3.5}$$

In this study, we use a modified form of equation 3.5 as

$$\frac{\langle \overline{u}_1 \rangle}{u_\tau} = \frac{1}{\kappa}\ln\left(\frac{x_3 - d}{L_3}\right) + \mathrm{B} - \frac{\Delta' u_1}{u_\tau} \,, \tag{3.6}$$

where $\Delta' u_1/u_\tau$ is a modified roughness function defined as

$$\frac{\Delta' u_1}{u_\tau} = \frac{\Delta u_1}{u_\tau} - \frac{1}{\kappa}\ln\left(\frac{L_3}{h}\right) \,. \tag{3.7}$$

For the smooth wall flow at high Reynolds numbers, values of κ and B are chosen as 0.384 and 4.17, respectively, as recommended by Monkewitz *et al.* (2008). Figure 13 depicts the mean streamwise velocity across multiple cases with varying packing densities and SSs. The solid black line serves as a reference to highlight the profile of smooth wall flow. The parallel deviations from the black line correspond to the magnitude of the modified roughness function. The matching of slope of the profiles with the reference line indicates the existence of an inertial sublayer. For the existence of logarithmic profiles, a layer sufficiently distant from the surface is necessary, such that the canopy scales do not impact the flow, and from the boundary layer height, such that L_3 is not a dominant length scale. Hence, SS becomes an

essential parameter to determine whether the characteristics of the true inertial sublayer can be retrieved. In this study, an upper limit of $0.15L_3$ is considered for the inertial sublayer as beyond this height, the boundary layer height L_3 becomes a dominant scale (Jiménez 2004; Marusic & Monty 2019). However, some researchers have recommended a larger value of $0.3L_3$ (Pope 2000). The dashed lines in Figure 13 indicate the upper limit of $0.15L_3$ for cases with $\lambda_p = 0.25$ and 0.062, and the colors correspond to the velocity profiles. The solid horizontal lines represent the height of the canopy in these cases.

Figure 13(a, b) shows that a logarithmic rise in the velocity is noticeable for cases with packing densities of 0.25 and 0.062 and SSs of 12 and 16. However, as the SS decreases to 8, the extent of the logarithmic layer is substantially reduced compared to the SSs of 12 and 16. For this SS, the logarithmic rise is only observed for the case with a packing density of 0.25 around the $0.15L_3$ mark. This occurs because the height extent of the RSL for a densely packed configuration (e.g., $\lambda_p = 0.25$) is smaller than that for configurations with relatively sparse arrangements (e.g., $\lambda_p = 0.062$), which can be observed from the extent to which the dispersive fluxes are significant (not shown). Hence, for the case with $\lambda_p = 0.25$, the extent of the RSL does not entirely occupy the significant portion of the region where the inertial sublayer can exist. However, the same is not true for the case with $\lambda_p = 0.062$. For cases with a SS of 4, the height of the canopy exceeds the upper limit of the extent of the inertial sublayer, and thus, the inertial sublayer is not observed for any case.

Cases with packing densities of 0.028 and 0.007 have been excluded from the above discussion because these configurations generate secondary flows (see § 3.3). The size and strength of the secondary flows are significantly influenced by the height of the boundary layer, as s_2/L_3 is one of the crucial parameters governing secondary flows. Thus, for the cases with secondary flows, the height of the boundary layer L_3 directly impacts the flow velocity in the RSL, which are occupied by the counter-rotating vortices. Consequently, if L_3 affects the velocity at the wall as well as near the top boundary, there is no layer in-between where the impact of L_3 on the velocity can be neglected. As a result, the basic requirement of independence from L_3 required for the existence of an inertial sublayer does not hold, and it comes as no surprise that we do not observe an inertial sublayer for these cases in figure 13. This behavior is consistent with findings from secondary flow research by Willingham *et al.* (2014).

These findings highlight a crucial aspect of canopy flows, where the existence of an inertial sublayer is not solely determined by the SS as in the case of smooth wall flows but also depends on the packing density of the underlying surface. Figure 13 illustrates that, for a given SS, the inertial sublayer may or may not exist depending on the underlying canopy configuration. Specifically, for a densely packed configuration, the flow may exhibit an inertial sublayer, while a sparsely arranged canopy may not exhibit such a layer for a particular SS.

4. Conclusion

In this study, we investigate the impact of numerical domain size on turbulent flow statistics for canopy flows spanning a wide range of packing densities. Specifically, we consider the impact of three relevant length scales: YAR (L_2/L_3), XAR (L_1/L_3), and SS (L_3/h). Furthermore, we explore the question of the existence of an inertial sublayer for a wide range of cases with different packing densities and scale separations. Our findings reveal that poorly designed domains can have a significant impact on turbulent flow statistics and turbulent coherent structures. We outline the main findings of this study as follows:

(i) Impact of cross-stream aspect ratio (L_2/L_3): Narrower domains, characterized by YAR considerably below 3.0, can be inadequate to accommodate a pair of fast and slow turbulent streaks, thereby artificially destroying the growth of turbulent structures in the streamwise
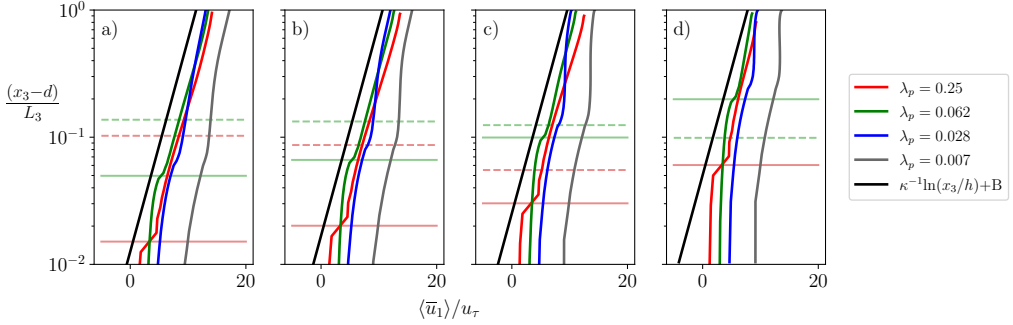
Figure 13: Mean streamwise velocity profiles for different scale separations, (a) 16, (b) 12, (c) 8, (d) 4. The vertical profiles for each scale separation correspond to different packing density cases mentioned in table 3, under the h scaling column. The horizontal lines correspond to the region between canopy height ($x_3/h = 1$, solid) and the theoretical limit of the extent of inertial sublayer ($x_3/L_3 = 0.15$, dashed) for packing densities 0.25 and 0.062.

direction. Additionally, a decrease in the growth of cross-stream structures is observed by analyzing the integral length scale L_{22} in narrower domains. Moreover, the statistics indicate that narrower domains tend to underpredict the value of streamwise variance across a wide range of packing densities. Overall, it is concluded that domains with YAR 3.0 or more are sufficient to reduce the artificial impact of cross-stream periodization and to accurately capture the first and second-order statistics. Detailed information about the specific errors in first and second-order statistics in UCL, URSL, and OL can be found in table 4.

(ii) Impact of streamwise aspect ratio (L_1/L_3): Shorter domains, characterized by XAR considerably below 6.0, experience excessive periodization, resulting in an artificial strength-ening of the turbulent coherent structures in the streamwise direction. As a result, the coherent structures may exhibit longer correlation values throughout the domain. Additionally, the statistics reveal that the shorter domains tend to overpredict the value of streamwise variance across a wide range of packing densities. Overall, it is determined that domains with XAR 6.0 or more are sufficient to reduce the artificial impact of streamwise periodization and to accurately capture the first and second-order statistics. Detailed information about the specific errors in first and second-order statistics in UCL, URSL, and OL can be found in table 5.

(iii) Impact of scale separation (L_3/h): This study demonstrates that the conventional method to test the impact of scale separation has major limitations for canopy flows, especially for configurations where the parameter s_2/L_3 exceeds 0.5. To overcome the limitations of the existing method, a new set of Pi groups is proposed that can relatively accurately isolate the effects of scale separation. Using the novel L_3 scaling approach, we observe that domains with limited scale separation tend to underestimate the variance values in the outer layer. In addition, our findings reveal that a scale separation of 12 and above is adequate to reduce the artificial impact of the top boundary condition on flow statistics in the UCL, URSL, and till, up to at least $0.6L_3$ in the OL. Detailed information about the specific errors in first and second-order statistics can be found in table 6 and 7.

(iv) Existence of inertial sublayer: Conventionally, scale separation is considered the sole parameter to determine the presence of an inertial sublayer in a flow field. However, our study shows that for canopy flows, the existence of an inertial sublayer depends not only on scale separation but also on the arrangement of the underlying surface. This is because the extent of the RSL depends on the underlying surface configuration and also because

24

705 certain arrangements generate secondary flows which occupy the entire RSL. We found
706 that for moderately dense ($\lambda_p = 0.062$) and dense ($\lambda_p = 0.25$) cases, a logarithmic rise in
707 the streamwise velocity profile could be recovered for scale separations of 12 and beyond.
708 However, for a scale separation of 8, only the densely packed case ($\lambda_p = 0.25$) exhibited the
709 characteristic logarithmic rise. For sparse configurations which generate secondary flows, it is
710 observed that the inertial sublayer does not exist for any scale separation. Scaling justification
711 is provided in order to support the observed results for secondary flow cases.

712   Overall, our results indicate that a domain with an SS of 12 or larger, YAR of 3.0 or larger,
713 and XAR of 6.0 or larger is suitable for minimizing the artificial impacts of the numerical
714 domain. However, researchers can use the error values reported in tables 4, 5, 6 and 7 to
715 choose smaller domain than recommended based on their region of interest and research
716 purpose. It is important to note that our study only considers the aligned configuration of
717 canopy elements, but we expect our recommendations to be valid for staggered as well
718 as other configurations based on the physical justifications provided in each section. We
719 recommend that researchers match their configurations with an aligned configuration that
720 has a similar extent of RSL.

731 **Appendix A.**

732 This section presents an analysis of the influence of grid resolution on turbulent flow statistics,
733 specifically on streamwise velocity, streamwise variance, and Reynolds shear stress. To
734 conduct this study, a computational domain with SS of 4, YAR of 4.5, and XAR of 6.0
735 is selected. The domain is discretized with different resolutions such that $n_1 \times n_2 \times n_3 =$
736 $4 \times 4 \times 8, 6 \times 6 \times 12, 8 \times 8 \times 16$, where n_i represents the number of collocation nodes per
737 cube edge. Although this domain is not sufficient to accurately capture the turbulent flow
738 statistics, the aim of this section is to demonstrate that the flow field is not significantly
739 impacted by the choice of grid resolution, indicating that the chosen domain is appropriate
740 for this purpose. The results presented in figure 14 reveal that the resolutions of $4 \times 4 \times 8$
741 and $6 \times 6 \times 12$ can predict the trends in the profiles with satisfactory accuracy based on the
742 scope of this work. The errors associated with these profiles are summarized in table 8. Error
743 values are modest compared to corresponding variations in flow statistics resulting from
744 XAR, YAR, and SS. Since the existence of the inertial sublayer necessitates the accurate
745 capture of flow statistics, a higher resolution of $6 \times 6 \times 12$ is selected for the analysis of the
746 impact of scale separation in §3.3. For §3.1 and 3.2, a lower resolution of $4 \times 4 \times 8$ is chosen
747 to ensure the computational feasibility of this study.

REFERENCES

748 ALBERTSON, J. D. & PARLANGE, M. B. 1999*a* Natural integration of scalar fluxes from complex terrain. *Adv.*
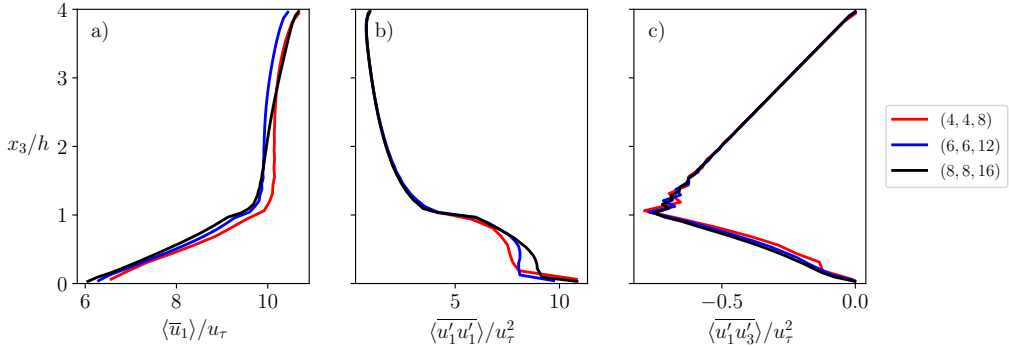749   *Water Resour.* **23**, 239–252.

Figure 14: (a) Streamwise velocity, (b) streamwise variance and (c) Reynolds shear stress profiles for a case with a packing density of 0.028, scale separation of 4, and an aspect ratio of 1 : 4.5 : 6, at different resolutions. The legend denotes the resolution as (n_1, n_2, n_3), where n_i represents the number of collocation nodes per cube edge.

resolution	$\langle \overline{u}_1 \rangle / u_\tau$	$\langle \overline{u_1' u_1'} \rangle / u_\tau^2$	$\langle \overline{u_1' u_3'} \rangle / u_\tau^2$
$4 \times 4 \times 8$	0.0292	0.0919	0.0538
$6 \times 6 \times 12$	0.0183	0.0687	0.0269

Table 8: Relative error (l_2 norm) of mean streamwise velocity, mean streamwise variance and Reynolds shear stress for different resolutions. Results from the case with the highest resolution ($8 \times 8 \times 16$) are considered to be ground truths.

ALBERTSON, J. D. & PARLANGE, M. B. 1999b Surface length scales and shear stress: Implications for land-atmosphere interaction over complex terrain. *Water Resour. Res.* **35**, 2121–2132.

ANDERSON, WILLIAM 2016 Amplitude modulation of streamwise velocity fluctuations in the roughness sublayer: evidence from large-eddy simulations. *Journal of Fluid Mechanics* **789**, 567–588.

ANDERSON, W., LI, Q. & BOU-ZEID, E. 2015 Numerical simulation of flow over urban-like topographies and evaluation of turbulence temporal attributes. *J. Turbul.* **16**, 809–831.

ANDREAS, E. L., CLAFFY, K. J., JORDAN, R. E., FAIRALL, C. W., GUEST, P. S., PERSSON, P. O. G. & GRACHEV, A. A. 2006 Evaluations of the von kármán constant in the atmospheric surface layer. *J. Fluid Mech.* **559**, 117–149.

BARLOW, J. F., HARMAN, I. N. & BELCHER, S. E. 2004 Scalar fluxes from urban street canyons. part i: Laboratory simulation. *Boundary-Layer Meteorol.* **113**, 369–385.

BOU-ZEID, E., MENEVEAU, C. & PARLANGE, M. B. 2005 A scale-dependent lagrangian dynamic model for large eddy simulation of complex turbulent flows. *Phys. Fluids* **17**, 025105.

BUCKINGHAM, E. 1914 On physically similar systems; illustrations of the use of dimensional equations. *Phys. Rev.* **4**, 345–376.

CANUTO, C., HUSSAINI, M. Y., QUARTERONI, A. & ZANG, T. A. 2007 *Spectral methods: evolution to complex geometries and applications to fluid dynamics*. Springer Science & Business Media.

CHAMECKI, M., MENEVEAU, C. & PARLANGE, M. B. 2009 Large eddy simulation of pollen transport in the atmospheric boundary layer. *J. Aerosol Sci.* **40**, 241–255.

CHESTER, S., MENEVEAU, C. & PARLANGE, M. B. 2007 Modeling turbulent flow over fractal trees with renormalized numerical simulation. *J. Comput. Phys.* **225**, 427–448.

CHUNG, D., HUTCHINS, N., SCHULTZ, M. P. & FLACK, K. A. 2021 Predicting the Drag of Rough Surfaces. *Annu. Rev. Fluid Mech.* **53**, 439–471.

CHUNG, D., MONTY, J. P. & HUTCHINS, N. 2018 Similarity and structure of wall turbulence with lateral wall shear stress variations. *J. Fluid Mech.* **847**, 591–613.

CLAUS, J., COCEAL, O., THOMAS, T. GLYN, BRANFORD, S., BELCHER, S. E. & CASTRO, I. P. 2012 Wind-Direction Effects on Urban-Type Flows. *Boundary-Layer Meteorol.* **142**, 265–287.

26

777 COCEAL, O., DOBRE, A., THOMAS, T. G. & BELCHER, S. E. 2007 Structure of turbulent flow over regular
778   arrays of cubical roughness. *J. Fluid Mech.* **589**, 375–409.

779 COCEAL, O., THOMAS, T. G., CASTRO, I. P. & BELCHER, S. E. 2006 Mean flow and turbulence statistics over
780   groups of urban-like cubical obstacles. *Boundary-Layer Meteorol.* **121**, 491–519.

781 COMTE-BELLOT, G. 1963 *Contribution à l'étude de la turbulence de conduite.* impr. Guirimand.

782 FANG, J. & PORTÉ-AGEL, F. 2015 Large-eddy simulation of very-large-scale motions in the neutrally stratified
783   atmospheric boundary layer. *Boundary-Layer Meteorol.* **155**, 397–416.

784 FERNANDO, H., LEE, S.M., ANDERSON, J., PRINCEVAC, MARKO, PARDYJAK, ERIC & GROSSMAN-CLARKE,
785   SUSANNE 2001 Urban fluid mechanics: Air circulation and contaminant dispersion in cities. *Environ.*
786   *Fluid Mech.* **1**, 107–164.

787 GANAPATHISUBRAMANI, B., HUTCHINS, N., HAMBLETON, W. T., LONGMIRE, E. K. & MARUSIC, I. 2005
788   Investigation of large-scale coherence in a turbulent boundary layer using two-point correlations. *J.*
789   *Fluid Mech.* **524**, 57–80.

790 GIOMETTO, M. G., CHRISTEN, A., MENEVEAU, C., FANG, J., KRAFCZYK, M. & PARLANGE, M. B. 2016
791   Spatial characteristics of roughness sublayer mean flow and turbulence over a realistic urban surface.
792   *Boundary-Layer Meteorol.* **160**, 425–452.

793 GORLÉ, C., GARCIA-SANCHEZ, C. & IACCARINO, G. 2015 Quantifying inflow and rans turbulence model form
794   uncertainties for wind engineering flows. *J. Wind. Eng. Ind.* **144**, 202–212.

795 JIMÉNEZ, J. 2004 Turbulent flows over rough walls. *Annu. Rev. Fluid Mech.* **36**, 173–196.

796 KANDA, M., MORIWAKI, R. & KASAMATSU, F. 2004 Large-eddy simulation of turbulent organized structures
797   within and above explicity resolved cube arrays. *Boundary-Layer Meteorol.* **112**, 343–368.

798 KIM, J. & MOIN, P. 1985 Application of a fractional-step method to incompressible navier-stokes equations.
799   *J. Comput. Phys.* **59**, 308–323.

800 LEONARDI, S. & CASTRO, I. P. 2010 Channel flow over large cube roughness: a direct numerical simulation
801   study. *J. Fluid Mech.* **651**, 519–539.

802 LI, Q., BOU-ZEID, E., ANDERSON, W., GRIMMOND, S. & HULTMARK, M. 2016 Quality and reliability of les
803   of convective scalar transfer at high reynolds numbers. *Int. J. Heat Mass Transf.* **102**, 959–970.

804 LOWE, D., EBI K. L. & FORSBERG, B. 2011 Heatwave early warning systems and adaptation advice to reduce
805   human health consequences of heatwaves. *Int. J. Environ. Res. Public Health* **8**, 4623–4648.

806 LOZANO-DURÁN, A. & JIMÉNEZ, J. 2014 Effect of the computational domain on direct simulations of turbulent
807   channels up to $Re\tau = 4200$. *Phys. Fluids* **26**.

808 MARGAIRAZ, F., GIOMETTO, M. G., PARLANGE, M. B. & CALAF, M. 2018 Comparison of dealiasing schemes
809   in large-eddy simulation of neutrally stratified atmospheric flows. *Geosci. Model Dev.* **11**, 4069–4084.

810 MARUSIC, I. & MONTY, J. P. 2019 Attached eddy model of wall turbulence. *Annu. Rev. Fluid Mech.* **51**,
811   49–74.

812 MEILI, N., MANOLI, G., BURLANDO, P., BOU-ZEID, E., CHOW, W. T. L., COUTTS, A. M., DALY, E., NICE, K. A.,
813   ROTH, M., TAPPER, N. J., VELASCO, E., VIVONI, E. R. & FATICHI, S. 2020 An urban ecohydrological
814   model to quantify the effect of vegetation on urban climate and hydrology (ut&c v1.0). *Geosci. Model*
815   *Dev.* **13**, 335–362.

816 MITTAL, R. & IACCARINO, G. 2005 Immersed boundary methods. *Annu. Rev. Fluid Mech.* **37**, 239–261.

817 MOIN, P. & KIM, J. 1982 Numerical investigation of turbulent channel flow. *J. Fluid Mech.* **118**, 341–377.

818 MOMEN, M. & BOU-ZEID, E. 2017 Mean and turbulence dynamics in unsteady ekman boundary layers. *J.*
819   *Fluid Mech.* **816**, 209–242.

820 MONKEWITZ, P. A., CHAUHAN, K. A. & NAGIB, H. M. 2008 Comparison of mean flow similarity laws in zero
821   pressure gradient turbulent boundary layers. *Phys. Fluids* **20**, 105102.

822 OKE, T. R. 1982 The energetic basis of the urban heat island. *Q. J. R. Meteorol. Soc.* **108**, 1–24, arXiv:
823   https://rmets.onlinelibrary.wiley.com/doi/pdf/10.1002/qj.49710845502.

824 OKE, T. R., MILLS, G., CHRISTEN, A. & VOOGT, J. A. 2017 *Urban Climates.* Cambridge University Press.

825 ORSZAG, S. A. 1970 Analytical theories of turbulence. *J. Fluid Mech.* **41**, 363–386.

826 ORSZAG, S. A. & PAO, Y. 1975 Numerical computation of turbulent shear flows. In *Adv. Geophys.*, , vol. 18,
827   pp. 225–236. Elsevier.

828 PHILIPS, D. A., ROSSI, R. & IACCARINO, G. 2013 Large-eddy simulation of passive scalar dispersion in an
829   urban-like canopy. *J. Fluid Mech.* **723**, 404–428.

830 POPE, S. B. 2000 *Turbulent flows.* Cambridge University Press.

831 RAUPACH, M. R., ANTONIA, R. A. & RAJAGOPALAN, S. 1991 Rough-wall turbulent boundary layers. *Appl.*
832   *Mech. Rev.* **44**, 1–25.

833 ROTACH, M. W. 1993 Turbulence close to a rough urban surface part I: Reynolds stress. *Boundary-Layer*
834   *Meteorol.* **65**, 1–28.

835 ROTACH, M. W. 1999 On the influence of the urban roughness sublayer on turbulence and dispersion.
836   *Atmospheric Environment* **33**, 4001–4008.

837 ROTACH, M. W., VOGT, R., BERNHOFER, C., BATCHVAROVA, E., CHRISTEN, A., CLAPPIER, A., FEDDERSEN,
838   B., GRYNING, S., MARTUCCI, G., MAYER, H. & OTHERS 2005 Bubble–an urban boundary layer
839   meteorology project. *Theor. Appl. Climatol.* **81**, 231–261.

840 SALESKY, S. T., CALAF, M. & ANDERSON, W. 2022 Unstable turbulent channel flow response to spanwise-
841   heterogeneous heat fluxes: Prandtl's secondary flow of the third kind. *J. Fluid Mech.* **934**, A46.

842 SALESKY, S. T., CHAMECKI, M. & BOU-ZEID, E. 2017 On the nature of the transition between roll and cellular
843   organization in the convective boundary layer. *Boundary-Layer Meteorol.* **163**, 41–68.

844 SCHMID, M. F., LAWRENCE, G. A., PARLANGE, M. B. & GIOMETTO, M. G. 2019 Volume Averaging for Urban
845   Canopies. *Boundary-Layer Meteorol.* **173**, 349–372.

846 SCHUMANN, U. 1973 *Ein Verfahren zur direkten numerischen Simulation turbulenter Strömungen in Platten-*
847   *und Ringspaltkanälen und über seine Anwendung zur Untersuchung von Turbulenzmodellen.* Ges. f.
848   Kernforschung mbH.

849 STROH, A., SCHÄFER, K., FROHNAPFEL, B. & FOROOGHI, P. 2020 Rearrangement of secondary flow over
850   spanwise heterogeneous roughness. *J. Fluid Mech.* **885**, 1–12, arXiv: 1910.07205.

851 TOMKINS, C. D. & ADRIAN, R. J. 2003 Spanwise structure and scale growth in turbulent boundary layers. *J.*
852   *Fluid Mech.* **490**, 37–74.

853 VANDERWEL, C. & GANAPATHISUBRAMANI, B. 2015 Effects of spanwise spacing on large-scale secondary
854   flows in rough-wall turbulent boundary layers. *J. Fluid Mech.* **774**.

855 WANG, Z., BOU-ZEID, E., AU, S. K. & SMITH, J. A. 2011 Analyzing the sensitivity of wrf's single-layer urban
856   canopy model to parameter uncertainty using advanced monte carlo simulation. *J. Appl. Meteorol.*
857   *Climatol.* **50**, 1795 – 1814.

858 WANGSAWIJAYA, D. D., BAIDYA, R., CHUNG, D., MARUSIC, I. & HUTCHINS, N. 2020 The effect of spanwise
859   wavelength of surface heterogeneity on turbulent secondary flows. *J. Fluid Mech.* .

860 WILLINGHAM, D., ANDERSON, W., CHRISTENSEN, K. T. & BARROS, J. M. 2014 Turbulent boundary layer flow
861   over transverse aerodynamic roughness transitions: Induced mixing and flow characterization. *Phys.*
862   *Fluids* **26**, 025111.

863 XIE, Z. & CASTRO, I. P. 2006 LES and RANS for turbulent flow over arrays of wall-mounted obstacles. *Flow*
864   *Turbul. Combust.* **76**, 291–312.

865 XIE, Z., COCEAL, O. & CASTRO, I. P. 2008 Large-eddy simulation of flows over random urban-like obstacles.
866   *Boundary-Layer Meteorol.* **129**, 1–23.

867 YANG, J. & ANDERSON, W. 2017 Numerical Study of Turbulent Channel Flow over Surfaces with Variable
868   Spanwise Heterogeneities: Topographically-driven Secondary Flows Affect Outer-layer Similarity
869   of Turbulent Length Scales. *Flow Turbul. Combust.* **100**, 1–17.

870 YANG, X. I. A. 2016 On the mean flow behaviour in the presence of regional-scale surface roughness
871   heterogeneity. *Boundary-Layer Meteorol.* **161**, 127–143.

872 YANG, X. I. A. & MENEVEAU, C. 2016 Recycling inflow method for simulations of spatially evolving turbulent
873   boundary layers over rough surfaces. *J. Turbul.* **17**, 75–93.

874 ZHANG, WEN, ZHU, XIAOWEI, YANG, XIANG I A & WAN, MINPING 2022 Evidence for raupach et al.'s
875   mixing-layer analogy in deep homogeneous urban-canopy flows. *Journal of Fluid Mechanics* **944**,
876   A46.

877 ZHENG, X., MONTAZERI, H. & BLOCKEN, B. 2021 Large-eddy simulation of pollutant dispersion in generic
878   urban street canyons: Guidelines for domain size. *J. Wind. Eng. Ind.* **211**, 104527.